JACS
JOURNAL OF THE AMERICAN CHEMICAL SOCIETY
pubs.acs.org/JACS
Article

Cell-Selective Multifunctional Surface Covalent Reconfiguration Using Aptamer-Enabled Proximity Catalytic Labeling

Yuna Guo,[#] Nan Wang,[#] Yihong Zhong,[#] Wei Li, Yiran Li, Guyu Wang, Yunyan Yao, Yue Shi, Liusheng Chen, Xiaojian Wang, Lin Ding,* and Huangxian Ju

Cite This: J. Am. Chem. Soc. 2023, 145, 5092−5104
Read Online
ACCESS | Metrics & More | Article Recommendations | Supporting Information

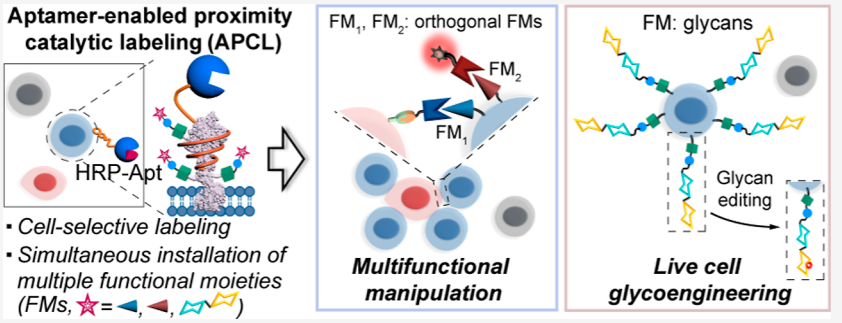

ABSTRACT: Cell surface engineering provides access to custom-made cell interfaces with desirable properties and functions. However, cell-selective covalent labeling methods that can simultaneously install multiple molecules with different functions are scarce. Herein, we report an aptamer-enabled proximity catalytic covalent labeling platform for multifunctional surface reconfiguration of target cells in mixed cell populations. By conjugating peroxidase with cell-selective aptamers, the probes formed can selectively bind target cells and catalyze target-cell-localized covalent labeling *in situ*. The universal applicability of the platform to different phenol-modified functional molecules allows us to perform a variety of manipulations on target cells, including labeling, tracking, assembly regulation, and surface remodeling. In particular, the platform has the ability of multiplexed covalent labeling, which can be used to install two mutually orthogonal click reactive molecules simultaneously on the surface of target cells. We thus achieve "multitasking" in complex multicellular systems: programming and tracking specific cell−cell interactions. We further extend the functional molecules to carbohydrates and perform ultrafast neoglycosylation on target living cells. These newly introduced sugars on the cell membrane can be recognized and remodeled by a glycan-modifying enzyme, thus providing a method package for cell-selective engineering of the glycocalyx.

INTRODUCTION

Biological processes usually take place through the delicate cooperation of multiple types of cells. In these processes, the molecular components of the cell membrane dictate how the cell interacts with its surroundings.[1] *In situ* surface remodeling of cells of interest in complex systems is essential for understanding and applying the mechanisms of life processes. Through selective labeling of the target cells, these cells can be distinguished,[2,3] and the cellular signaling pathways can be revealed with the aid of quantitative proteomics and single-cell sequencing technologies.[4,5] However, by introducing recognition molecules on the surface of target cells,[6−8] we can endow specific cells with sensing ability, regulate cellular functions, and reprogram cell−cell communication or interaction *in situ* in real biological systems, which have great application prospects in building synthetic tissues,[9−12] constructing artificial signaling pathways,[13] guiding immune cell targeting, and so forth.[14−16]

Although genetic engineering is the dominant method for accurately indicating target cells (through fluorescent protein fusion)[17] and rewiring cell−cell assembly (by the expression of cadherins,[11] adhesins,[18] coiled coils,[12] *etc.*), most of these works need to label/modify separate target cells prior to mixing different cell types. In addition, the genetic payload that we can reliably deliver is limited.[19] Therefore, covalent installation of functional molecules using nongenetic methods from the outside of cells is an attractive alternative for reconfiguring the cell membrane. Covalent conjugation possesses superior properties over noncovalent counterparts including prolonged residence time, higher biochemical

Received: October 20, 2022
Published: February 23, 2023

https://doi.org/10.1021/jacs.2c11150
J. Am. Chem. Soc. 2023, 145, 5092−5104

Scheme 1. Schematics of the APCL Strategy[a]

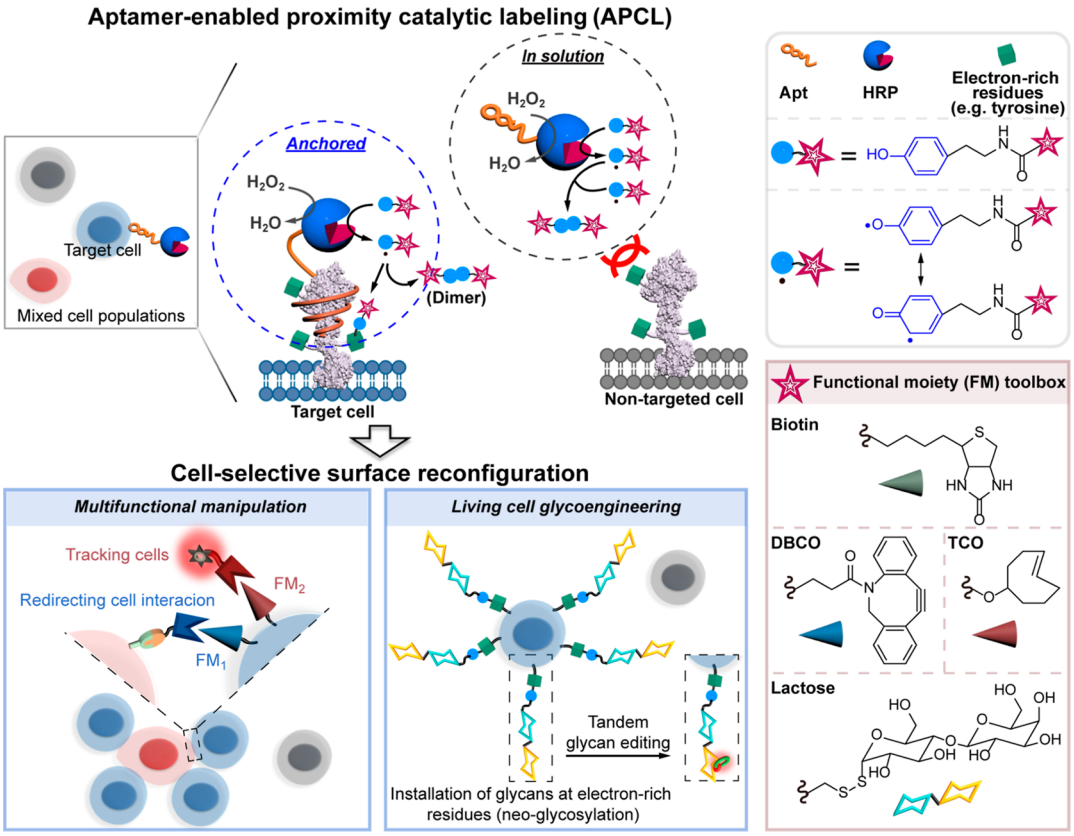

[a]HRP-Apt can specifically bind target cells in mixed cell populations and mediate cell-selective covalent labeling of various phenol-modified functional molecules, which enables multifunctional manipulation and glycocalyx remodeling of living cells.

efficiency and potency, and reduced dosage.[20−22] On one hand, it has been shown to selectively label target cells *in situ* in mixed cell populations.[2] On the other hand, it theoretically allows the simultaneous introduction of many different functional molecules into a given cell membrane, with little restriction on the number of molecular species.

At present, the state-of-the-art covalent labeling strategies with spatial specificity from outside of cells mainly include two categories: (1) genetically fusing peroxidases (APEX,[23] APEX2,[24] or HRP[25]) or biotin ligases (BioID[26] and TurboID[27]) to a target region, which can catalyze the covalent labeling to proximal proteins[28,29] and (2) using affinity recognition to drive covalent labeling to occur at specific locations.[2,30−42]

In a groundbreaking approach by MacMillan *et al.*, Ir complex-conjugated antibodies were utilized for spatially localizing carbene generation to map the microenvironment of immune cells.[39] However, most of these methods are designed for making a single type of labeling on the cell membrane and with the purpose of deciphering molecular interactions. We believe that if different types of functional molecules can be covalently mounted on the surface of target cells at the same time, the flexibility of cell manipulation and multifunctional integration ability will be greatly improved so as to expand the application field of target cell labeling technology. However, strategies that allow simultaneous covalent installation of different molecules onto specific cells are scarce. In addition, current methods mainly explore the labeling of biotin, fluorophores, or bio-orthogonal groups that can achieve click reaction but do not pay attention to the selective covalent mounting of complex biomolecules on target cells.

We thus identified a series of design requirements to achieve multifunctional remodeling of the target cell surface: an aptamer (Apt) was selected as the targeting moiety[30−32] to localize the labeling module due to the exquisite affinity and specificity for target cells and the small size.[43] These short single-stranded nucleic acid molecules can be obtained by powerful selection strategies and automated chemical synthesis,[44] and they can easily achieve site-specific chemical modification. Unlike the few current aptamer-driven proximity labeling methods, in which only one label can be generated by one recognition,[30−32] we design to couple Apt with a HRP-based catalytic labeling module to achieve cyclic and multiplexed covalent labeling. HRP can mediate the transformation of phenol-containing molecules to highly reactive, short-lived (<1 ms), and proximally restricted (<20 nm) phenoxy radicals,[23] which can covalently link to neighboring electron-rich residues [tyrosine (Tyr), tryptophan (Trp), *etc.*], thus allowing labeling to be restricted to target cells.[37] Furthermore, by linking tyramine to different functional moieties, phenol-containing molecules can be simply synthesized in a modular manner.[29]

Herein, we report an aptamer-enabled proximity catalytic labeling (APCL) platform for cell-selective multifunctional surface reconfiguration in mixed cell populations (Scheme 1). We carefully investigate the labeling process and attribute the cell selectivity to the increased local concentration of phenoxy radicals on the surface of target cells by Apt, as well as the short lifetime of phenoxy radicals. Compared with labeling

https://doi.org/10.1021/jacs.2c11150
J. Am. Chem. Soc. 2023, 145, 5092−5104

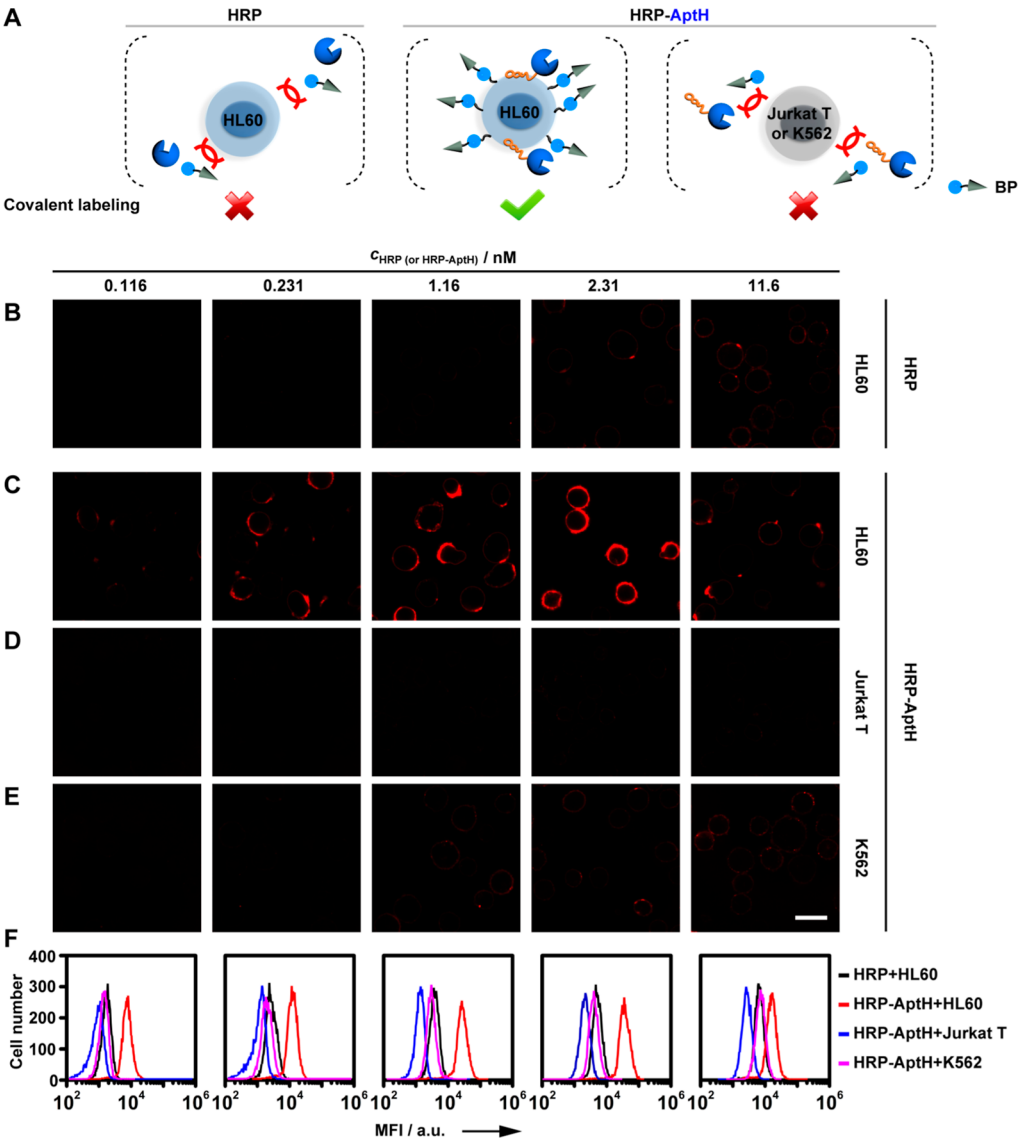

Figure 1. Investigation of the labeling performance of HRP-AptH and HRP on various cell lines. (A) Schematic diagram of the different labeling outcomes of HRP-AptH and HRP. CLSM (B–E) and FCM (F) analysis of the BP labeling extent on different cell lines undergoing HRP-AptH (or HRP) incubation in the presence of BP and H_2O_2 and then SA-Cy3 staining. Scale bar: 20 μm. The images are representative of three individual experiments.

based on Apt affinity binding, the proposed method has a stronger ability to discriminate specific cells in complex systems. The APCL strategy is applicable to different Apt-cell pairs and diverse phenol-containing molecules and is capable of introducing different functional moieties on target cells at the same time. We exploit these features to redirect cell–cell interaction *in vitro*, and in particular, by incorporating two mutually orthogonal functional moieties on the surface of the target cell, we achieve simultaneous programing and tracking of cell assembly in a mixed-cell environment. Interestingly, we extend the application of APCL to a phenol-modified disaccharide by devising a peroxidase-mediated, living cell-compatible, ultrafast neoglycosylation strategy. This enables cell-selective glycoengineering at electron-rich amino acid residues.

RESULTS AND DISCUSSION

Synthesis and Characterization of the APCL Probes. The peroxidase-based proximity labeling represents a powerful tool for profiling the proteome information of spatially specific biological regions.[23−25,35−37] In these strategies, the enzymes are introduced into biosystems by either (1) genetically expressing the enzyme at the designated location of cells[23−25] or (2) functionalizing the enzyme with a targeting molecule (antibodies, *etc.*) for binding to a specific location followed by a washing step to remove unbound enzyme conjugates.[35−37] The labeling mechanism of cell membrane-anchored HRP has been well described in the literature.[45,46] In brief, taking biotin-phenol (BP) as the model, in the presence of H_2O_2, HRP can catalyze the transformation of phenolic hydroxyls of both BP in solution and Tyr in neighboring proteins to radicals.[46] Then, the free BP radical ($BP^{\bullet}$) can either react with a cell-exposed Tyr radical ($Tyr^{\bullet}$) to form a BP-Tyr linkage or be consumed by another $BP^{\bullet}$ in solution to yield a BP–BP dimer. However, whether freely diffused peroxidase conjugates affect the spatial specificity of labeling has been largely overlooked, and it is unclear whether enzymes mounted on target cells can label

https://doi.org/10.1021/jacs.2c11150
J. Am. Chem. Soc. 2023, 145, 5092−5104

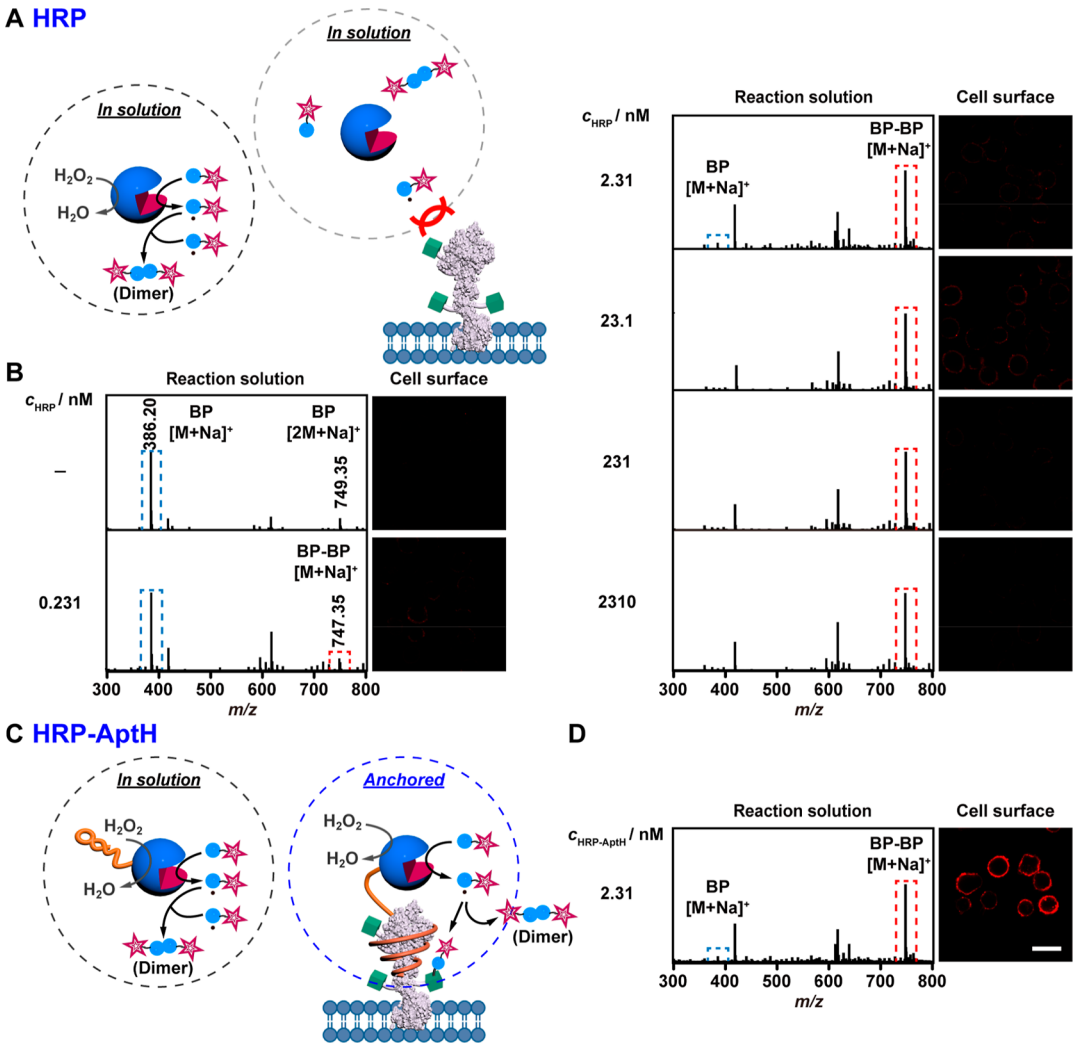

Figure 2. Investigation of the labeling mechanism of HRP-AptH and HRP. (A) Scheme showing the catalytic reaction mechanism of freely diffused HRP. (B) Left, ESI MS analysis of the mixture of HRP of different concentrations, BP and H_2O_2, after reaction for 3 min; right, CLSM imaging of cells after incubation with HRP of different concentrations for 1 h and 3 min reactions with BP and H_2O_2 and SA-Cy3 staining. (C) Scheme showing the catalytic reaction mechanism of freely diffused and cell-anchored HRP-AptH. (D) HRP-AptH (2.31 nM) was used to replace HRP in (B). Scale bar: 20 μm. The images are representative of three individual experiments.

nontargeted cells in mixed cell suspensions (without cell−cell interactions).

To clarify these issues, we began our trial by conjugating HRP with Apt and compared the labeling behaviors between HRP and the HRP−Apt conjugate. We chose two types of Apt, KH1C12[47] (abbreviated as AptH) and T2-KK1B10[48] (abbreviated as AptK), as the models, which can specifically bind human leukemia cell lines HL60 and K562 cells, respectively. Accordingly, two types of HRP-Apt conjugates, HRP-AptH and HRP-AptK, were prepared using 4-(*N*-maleimidomethyl) cyclohexane-1-carboxylic acid 3-sulfo-*N*-hydroxysuccinimide ester (sulfo-SMCC) as a bifunctional linker (Figure S1A,B). The coupling of Apt with HRP was verified using sodium dodecyl sulfate−polyacrylamide gel electrophoresis (SDS-PAGE) (Figure S1C) and the UV−vis absorption assay (Figure S1D). We then used a typical Amplex Red enzyme assay to verify the maintained HRP activity in HRP−Apt conjugates (Figure S1E,F).

Investigation of the Labeling Mechanism of HRP−AptH. With HRP−Apt successfully prepared, we proceeded to compare the labeling performance of HRP and HRP−AptH toward HL60 cells. We first verified the binding specificity of AptH by incubating Cy3-labeled AptH (Cy3-AptH) with HL60 cells using K562 and Jurkat T (human T lymphocyte) as control suspension cells (Figure S2). After that, we incubated HL60 cells with HRP and HRP-AptH, respectively, for 60 min. Then, without washing, BP (200 μM) and H_2O_2 (400 μM) were added, followed by a 3 min incubation to accomplish the labeling. After quenching the reaction using NaN_3 and sodium ascorbate and removing excess BP by centrifugation, the extent of BP labeling on HL60 cells was assessed by staining BP with streptavidin-Cy3 (SA-Cy3) using confocal laser scanning microscopy (CLSM) imaging and flow cytometry (FCM) (Figure 1). HL60 cells in the HRP-AptH group displayed robust Cy3 fluorescence on the cell membrane, and the signal became greater with increasing HRP-AptH concentration ($c_{HRP-AptH}$, 0.116−2.31 nM) (Figures 1A,C,F and S3). However, replacement of HRP-Apt by HRP led to much weaker fluorescence (Figures 1A,B,F and S3). The successful labeling by HRP-AptH was demonstrated to be dependent on the presence of HRP-AptH, BP, and H_2O_2 (Figure S4).

https://doi.org/10.1021/jacs.2c11150
J. Am. Chem. Soc. 2023, 145, 5092−5104

To reveal the reason why freely diffused HRP could not label cells, two groups of experiments were performed: (1) mixing HRP of different concentrations (c_{HRP}, 0, 0.231, 2.31, 23.1, 231, and 2310 nM) with BP and H_2O_2, followed by monitoring of the reaction products using electrospray ionization mass spectrometry (ESI MS); (2) incubating HL60 cells with HRP in the same concentration range in the presence of BP and H_2O_2, followed by CLSM observation of the labeling signal on the cell surface (Figure 2A,B). The results showed that when c_{HRP} increased to more than 2.31 nM, the BP signal (m/z 386.2) disappeared, accordingly, BP−BP (m/z 747.35) was obviously generated (Figure 2B), indicating that HRP in solution could exhibit catalytic activity at more than 2.31 nM. In the investigated c_{HRP} range, which was basically higher than c_{HRP} used in Figure 1, negligible cell labeling could be observed (Figure 2B). These phenomena indicate that BP$^\bullet$ catalyzed by freely diffused HRP at concentrations lower than 2310 nM has a limited lifetime (<1 ms) and a short diffusion radius (<20 nM) and cannot reach the cell surface to react with Tyr (Figure 2A).[23,37] This rules out the possibility that freely diffused HRP can label cells. While in the case of HRP-AptH, owing to the confinement of HRP to HL60 cells by AptH, sufficient BP$^\bullet$ can be generated in close proximity to the cell surface, which, at least some of them, are capable of reacting with Tyr before being quenched by another BP$^\bullet$ in solution (Figure 2C,D). Because of that, elevating $c_{HRP\text{-}AptH}$ could drive the binding equilibrium between HRP-AptH with the cells, leading to a greater labeling signal (Figures 1C,F and S3). The maximal labeling level was obtained at a $c_{HRP\text{-}AptH}$ of 2.31 nM. However, when the $c_{HRP\text{-}AptH}$ was further elevated to 11.6 nM, the extent of labeling substantially decreased (Figures 1C,F and S3). This might be owing to the quenching of BP$^\bullet$, generated from cell-anchored HRP-AptH, by BP$^\bullet$ generated from the excessive, freely diffused HRP-AptH in solution. We also calculated the ratio of the mean fluorescence intensity (FI), from CLSM and FCM measurements, of the HRP-AptH group to the HRP group, which represented the labeling selectivity: the maximum ratio was obtained at a HRP-AptH (or HRP) concentration of 1.16 nM (Figure S5).

To further demonstrate our speculation, we performed two additional series of experiments: (1) we used two types of nontargeted cells, K562 and Jurkat T, to replace HL60 cells in the HRP-AptH labeling experiments. As expected, in the same $c_{HRP\text{-}Apt}$ range, a negligible labeling signal could be observed (Figures 1D−F and S3 and S5). The mean FI (MFI) ratio of HL60 cells relative to Jurkat T and K562 cells measured with FCM reached 21.4 and 9.0 at a $c_{HRP\text{-}AptH}$ of 1.16 nM, respectively (Figure S5B). (2) We incubated HL60 cells with 1.16 nM HRP or HRP-Apt in the presence of BP of different concentrations and 400 μM H_2O_2. Along with increasing BP concentration (c_{BP}) from 0 to 200 μM, the labeling extent increased for both HRP and HRP-AptH, while HRP-AptH displayed much more evident labeling than HRP (Figure S6). However, further increasing c_{BP} led to a significant decrease in labeling for either HRP-AptH or HRP. This could be attributed to the aggravated quenching probability of BP$^\bullet$, that is, BP−BP was generated as the dominant product. The optimal c_{BP} is thus chosen as 200 μM. Taken together, the above results indicate that the HRP-Apt conjugate can be used for specific covalent labeling of target cells, and the freely diffused conjugate in the cell suspension cannot label nontargeted cells (Figure 1A). The APCL operation only involves two times of reagent addition (I, HRP-AptH; II, BP + H_2O_2) and two short periods of incubation (1 h for HRP-AptH binding, 3 min for covalent labeling). We confirmed that the labeling reagents had good cytocompatibility and that the cells undergoing APCL remained active for a long time, rendering APCL ideally suited for the following live cell experiments (Figure S7). We further analyzed the BP-labeled proteins in HL60 cells by quantitative MS-based proteomics. The digested peptides of HRP-AptH- and HRP-treated samples were tagged by heavy (H) and light (L) dimethylation labeling reagents, respectively. In total, 35 proteins were significantly enriched ($\log_2$ (H/L) > 1), and 21 proteins were only labeled in HRP-AptH-treated HL60 cells with a maximal H/L ratio of 100, possibly associated with the binding sites of AptH to HL60 cells (Table S1).

To illustrate the advantages of using APCL to generate covalent labels, we compared the stability of BP generated by APCL with that of antibodies bound to cells by affinity recognition at the cell surface. Anti-B-cell lymphoma-2 antibody was used to specifically bind HL60 cells. We found that (1) BP covalently labeled by APCL was more stable in a weakly acidic environment (Figure S8); (2) after culturing labeled cells in RPMI-1640 complete medium for 4 or 8 h, the percentage of BP labeled by APCL staying on the cell surface was significantly higher than that of the antibody (Figure S9). The APCL technology uses affinity recognition to guide the occurrence of stable covalent labeling, providing a novel strategy for increasing the stability/residence time of surface modifications in engineered cells.

APCL in Mixed Cell Suspensions. We then proceeded to test APCL for the identification of specific cells in a more challenging system, that is, mixed cell suspensions. The model system was prepared by 1:1 mixing target HL60 cells with nontargeted K562 cells, which was abbreviated as H&K (H-to-K amount ratio, 1:1). K562 cells were prestained with membrane dye DiD (green) for cell identification. After performing APCL followed by SA-Cy3 staining, the CLSM images showed that only HL60 cells displayed Cy3 fluorescence (red) on the cell periphery (Figure 3A). The ratio of Cy3 MFI on HL60 to K562 cells (abbreviated as H-to-K MFI ratio) was estimated to be 6.9:1 using FCM. Using the FCM data, we also calculated the labeling efficiency (LE) of target cells by dividing the number of cells with $Cy3^+$ and DiD^- (Q4) by the number of cells with DiD^- (Q3 + Q4) and the labeling accuracy (LA) by dividing the number of cells with $Cy3^+$ and DiD^- (Q4) to the number of cells with $Cy3^+$ (Q1 + Q4). The LE and LA for the H&K system were 97.1 and 95.3%, respectively (Figure 3A). In comparison, replacement of HRP-AptH with HRP (LE, 0.9%) or omitting HRP-AptH (Control, LE, 0.1%) resulted in failure to label target cells (Figure 3A). The differentiation capability of APCL was also verified in a HL60-Jurkat T-mixed cell suspension (H&J) with a H-to-J amount ratio of 2:1 using HRP-AptH (Figure 3B). In agreement with the H&K system, APCL could distinguish HL60 and Jurkat T cells well: the H-to-J Cy3 MFI ratio was 10:1, and the LE and LA were 99.7 and 95.8%, respectively. To demonstrate the potential of APCL for *in vivo* experimental application, we also added 10 and 20% HL60 cells to peripheral blood mononuclear cells (PBMCs), and the results showed that APCL could selectively label HL60 cells (Figure S10). These results demonstrate that APCL has excellent LE and accuracy in the mixed-cell suspension system.

https://doi.org/10.1021/jacs.2c11150
J. Am. Chem. Soc. 2023, 145, 5092−5104

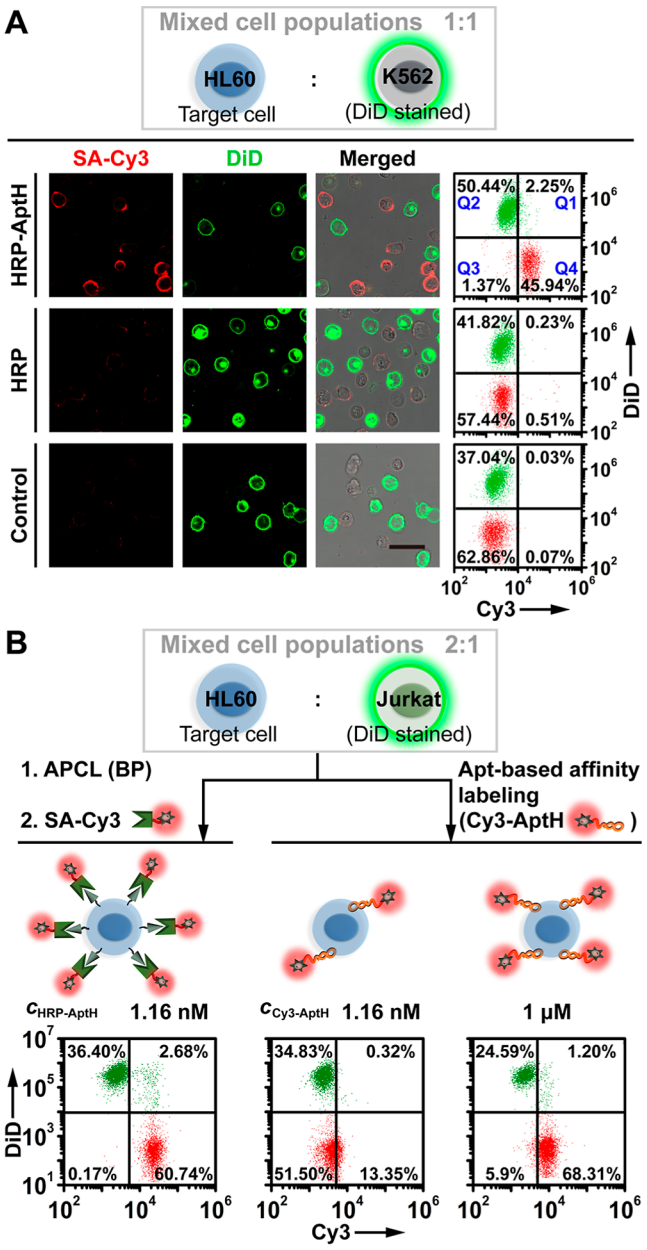

Figure 3. Demonstration of the cell selectivity for APCL in mixed cell suspensions. (A) CLSM imaging and FCM analysis of cell suspensions (target: HL60; nontargeted: K562; 1:1) undergoing HRP-AptH-based APCL. Control experiments were performed with HRP-AptH replaced by HRP or omitted. K562 cells were prestained with DiD (green), and BP was indicated by SA-Cy3 (red). Scale bar: 20 μm. (B) FCM comparison of the cell discriminative capability between APCL and direct Cy3-AptH labeling toward target HL60 and nontargeted Jurkat T cells (the amount ratio is 2:1). Jurkat T lymphocytes were prestained with DiD membrane dye (green), and BP was indicated using SA-Cy3 (red). For Cy3-AptH labeling, both the optimal concentration (1 μM) and the same concentration as HRP-AptH used for APCL were, respectively, used. The images are representative of three individual experiments.

We envisioned that APCL would transform one recognition event to multiple covalent labeling events, thus having better cell discrimination ability than noncovalent labeling based on exclusively Apt recognition. To demonstrate this, we treated the H&J suspension with Cy3-labeled AptH (Cy3-AptH) of the same concentration as HRP-AptH (2.27 nM) and the optimal concentration (1 μM), respectively (Figure 3B). The LE and differentiation in the two groups were significantly weaker than those in the APCL group: the LE was 20.6 and 92.0%, and the H-to-J Cy3 MFI ratio was 1.6:1 and 3.6:1, respectively. We also examined the ability of the anti-B-cell lymphoma-2 antibody to discriminate between the two cell types. The LE of antibody-based affinity labeling was 73.4%, and the H-to-J Cy3 MFI ratio was 3.2, both of which were significantly lower than the APCL method (Figure S11). These results highlight the significance of using the catalytic labeling feature of APCL for cell discrimination in mixed systems.

We further tested the discriminative performance of APCL in suspensions containing Jurkat T (nontargeted) and HL60 (target) cells in two ways: (1) dilution of the cell suspension at a constant J-to-H amount ratio (5:1). In the range of total cell concentration from 10^5 to 10^6 mL^{-1}, the discrimination effect was excellent (Figure S12A); (2) increasing the J-to-H amount ratio with the same number of HL60 cells (n_H). Even at a ratio of 10:1, the two cell types were still well discriminated, with a J-to-H Cy3 MFI ratio of 5.7:1 (Figure S12B). We also tested the cell-discriminating labeling ability of APCL in a mixed adherent cell system. Using HRP-AptM [AptM can specifically recognize mucin 1 (MUC1)] as the APCL probe, we successfully achieved BP labeling of MCF-7 cells in a coculture system of MUC1-positive MCF-7 cells and MUC1-negative HepG2 cells (Figure S13).

Extension of the Labeling Molecule Toolbox for APCL. Having demonstrated the feasibility of APCL, we were interested in whether the proposed method could be extended to other functional moieties. Installing different chemical handles on the cell surface will facilitate manipulation of the cell surface by allowing a diversity of cell membrane functions beyond those provided by natural evolution. Two widely used chemical moieties for click reactions, dibenzoazacyclooctyne (DBCO) and *trans*-cyclooctene (TCO), were chosen.[49] The complementary functionalities for the two moieties are N_3 and tetrazine (Tz), respectively. We first synthesized dibenzocyclooctyne-phenol (DP) and *trans*-cyclooctene-phenol (TP) by one-step ligation of DBCO-NHS and TCO-NHS with tyramine, respectively (Schemes S1 and S2). The products were characterized by ^{1}H NMR (Figures S14 and S15), ^{13}C NMR spectroscopy (Figures S16 and S17), and high-resolution mass spectrometry.

Using K562 as the model cell line and HRP-AptK as the APCL probe, we confirmed that DP and TP could be successfully installed on the cell surface through APCL using the complementary click reaction of N_3-Cy5 and Tz-Cy3, respectively (Figures S18 and S19). Similar to the BP labeling system, with the increase of DP (or TP) concentration, the labeling signal showed a trend of increase first and then decrease. The optimal concentrations for DP (Figure S18) and TP (Figure S19) were 200 and 400 μM, respectively. Again, freely diffused HRP failed to label cells regardless of DP (or TP) concentration. We further demonstrated in mixed cell suspensions (target: HL60; nontargeted: K562; prestained with PKH67) that DP (or TP) could be selectively labeled on cells mediated by HRP-AptH (Figure 4A). We further demonstrated in PBMCs that by using AptJ (an aptamer specifically targeting CD3ε) to construct the APCL probe, DP can be selectively labeled by APCL on CD3ε-positive cells and colocalized with the anti-CD3ε antibody (Figure S20). These data collectively suggest the general applicability of APCL to different phenol-modified molecules. This further encouraged

https://doi.org/10.1021/jacs.2c11150
J. Am. Chem. Soc. 2023, 145, 5092−5104

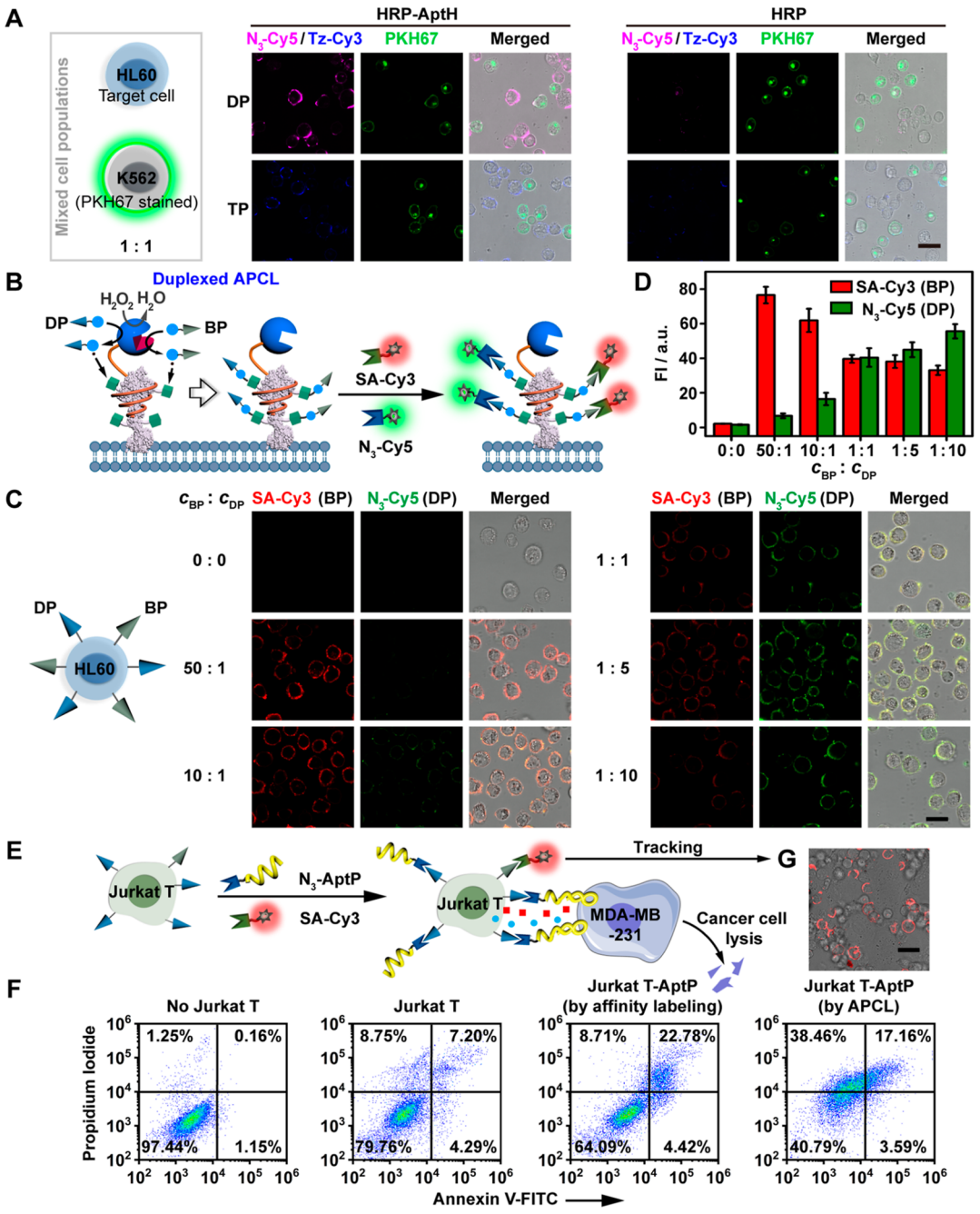

Figure 4. Duplexed APCL. (A) APCL labeling of target HL60 cells in mixed cell suspensions (HL60 + K562, 1:1) using DP or TP as the labeling molecules. As a control, HRP-AptH was replaced by HRP. K562 cells were prestained with PHK67 membrane dye (green), and cell surface-anchored DP and TP were indicated by N_3-Cy5 (purple) and Tz-Cy3 (blue), respectively. (B) Scheme showing the mechanism of duplexed APCL for mounting two types of labeling molecules on the same cell. (C) CLSM images of HL60 cells undergoing duplexed APCL using mixed labeling molecules (BP + DP, total concentration: 2 mM) with different BP-to-DP concentration ratios, followed by SA-Cy3 (indicating BP labeling) and N_3-Cy5 (indicating DP labeling) staining. (D) FI obtained from CLSM images in (C). (E) Schematic illustration of the preparation of AptP and Cy3 equipped, activated Jurkat T cells through duplexed APCL. Aptamer AptP can specifically bind PD-L1, thus bringing Jurkat T and PD-L1-positive MDA-MB-231 cells into proximity to boost cell killing. (F) FCM analysis of the apoptosis of MDA-MB-231 cells after incubation with activated Jurkat T cells, activated Jurkat T cells equipped with AptP by affinity labeling, and activated Jurkat T equipped with AptP and Cy3 by APCL for 6 h, respectively. (G) CLSM imaging of MDA-MB-231 cells after incubating with activated Jurkat T cells equipped with AptP and Cy3 by APCL for 2 h. Scale bars: 20 μm. The images are representative of three individual experiments, and data are presented as mean ± SD, n = 3.

us to try to introduce different types of molecules on the cell surface at the same time.

Simultaneous Installation of Dual Chemical Handles on Living Cells. To achieve multifaceted manipulation of cells, it is necessary to have the ability to customize functional groups on living cell membranes on demand.[14] However, multiplexed cell surface modification is challenging for most affinity-driven ligation techniques, some of which are limited by the labeling principle that a single probe can produce only one label[30−33] and others by the complex organic synthesis steps of labeling molecules.[38] In this regard, due to the catalytic nature of the labeling reaction, as well as its wide applicability

https://doi.org/10.1021/jacs.2c11150
J. Am. Chem. Soc. 2023, 145, 5092−5104

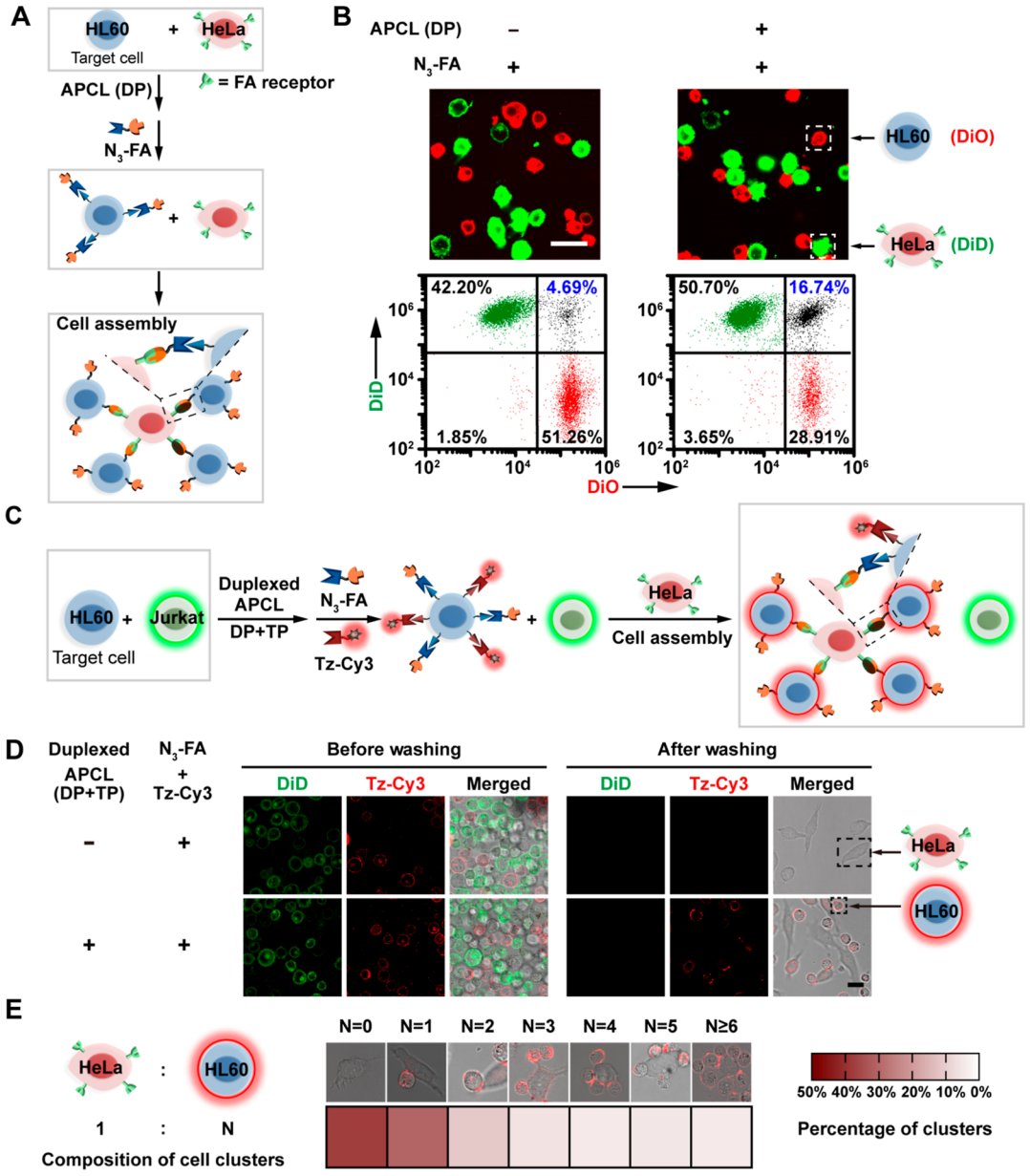

Figure 5. Programing of cell interactions using APCL. (A) Scheme for *in situ* redirection of the interaction between HL60 and HeLa cells in mixed cell suspensions by selective introduction of FA on HL60 cells using APCL and a secondary click reaction. (B) CLSM imaging and FCM analysis of the mixed cell suspension (HL60 + HeLa, 1:1) without and with APCL labeling of DP, followed by N_3-FA tagging and a 30 min incubation. HL60 cells were prestained with DiO (red), and HeLa cells were prestained with DiD (green). Scale bar: 20 μm. (C) Scheme for programming of the selective recruitment of HL60 cells by HeLa cell adhesion layer using duplexed APCL and mutually orthogonal click reactions. (D) After performing duplexed APCL (DP and TP) in mixed cell suspensions (HL60 + Jurkat T, 1:1), the cell mixture was allowed to react with the mixture of N_3-FA (to install FA on HL60 cells) and Tz-Cy3 (red, to indicate HL60 cells). CLSM images were obtained after incubating the prepared cell suspensions with HeLa adhesion cell layers immediately or after a washing step. Cell suspensions without duplexed APCL treatment were used as the control. Jurkat T cells were prestained with DiD (green). Scale bar: 20 μm. (E) Characterization of the formation of cell clusters. The percentage of clusters formed with 1 HeLa and 0, 1, 2, 3, 4, 5, and ≥6 HL60 cells was counted from the CLSM images. More than 100 HeLa cells were counted with ImageJ software. The images are representative of three individual experiments.

to phenol-modified molecules, APCL offers an ideal solution that operates much in the same way as single-channel labeling by simply mixing the desired labeling molecules together (Figure 4B).

To demonstrate this, we mixed BP and DP at different concentration ratios and then subjected HL60 cells to HRP-AptH-based APCL and used SA-Cy3 (red) and N_3-Cy5 (green) to indicate anchored BP and DP on the cells, respectively. CLSM imaging and FCM analysis revealed that both molecules were installed simultaneously on the cell surface (Figures 4C,D and S21). The intensity of each fluorescence channel was positively correlated with the proportion of corresponding labeled molecules (Figures 4D and S21B). These data demonstrate that our method can rapidly install both types of labeling molecules simultaneously and that the labeling ratio can be easily adjusted by changing the mixing ratio.

https://doi.org/10.1021/jacs.2c11150
J. Am. Chem. Soc. 2023, 145, 5092−5104

The simultaneously mounted BP and DP on cells can act as anchor points, allowing us to conveniently install different functional modules on the cells. To demonstrate this, we installed both BP and DP on activated Jurkat T cells by duplexed APCL (using HRP-AptJ; AptJ can specifically bind Jurkat T cells by recognizing CD3ε) and then mounted SA-Cy3 for fluorescence tracking of cells and N_3-AptP for specific binding to PD-L1-positive cells (Figure 4E). We found that the resulting engineered cells exhibited a significantly enhanced ability to kill PD-L1-expressing MDA-MB-231 cells compared to cells noncovalently assembled with DNA sequences consisting of AptJ and AptP ligated together and cells without AptP modification (Figures 4F and S22). This indicates that the synergistic effect of active targeting and blocking of PD1/PD-L1 by AptP may enhance the toxicity of the effector cells;[50] moreover, more AptP can be covalently and stably assembled on the cells through the "1:n" amplification modification of APCL, which further boosts the ability to kill tumor cells. The attachment of Jurkat T cells to MDA-MB-231 cells could be observed using Cy3 by CLSM (Figure 4G). This experiment shows the promise of using the covalent multilabeling ability of APCL to develop engineered cells for adoptive cell transfer-based therapies.

We further sought to take advantage of the cellular labeling specificity of APCL to mount different molecules to two different cell types separately. We designed a tandem APCL experiment using a mixed cell suspension of CCRF-CEM (CEM) and Ramos as the model: (1) performing APCL based on HRP-AptC (AptC can specifically bind CEM cells) to install BP on CEM cells; (2) releasing HRP-AptC from CEM cells by adding the complementary sequence of AptC; (3) performing APCL again based on HPR-AptR (AptR can specifically bind Ramos cells) to install DP on Ramos cells, thus enabling separate labeling of the two cell types (Figure S23).

Redirecting Intercellular Interactions. APCL provides a valuable tool for programing cell interactions in complex systems.[9,15,51−53] In biological systems, differentiated cells with discrete yet interdependent functions constitute multicellular organs to achieve higher-order functions.[9] Development of methods to direct cell−cell interactions will contribute to the revelation of the key mechanisms involved in complex developmental processes and offer great opportunities for the development of cell-based theranostics and tissue engineering.[54]

In this context, we first sought to manipulate the intercellular assembly of two originally noninteracting cell types in a mixed cell suspension (Figure 5A). The model cell lines consisted of target HL60 cells with negative folic acid (FA) expression, and nontargeted HeLa cells with high expression of FA receptor (FAR) (Figure S24).[55] We prestained HL60 cells with DiO (red) and HeLa cells with DiD (green) and then mixed them at an amount ratio of 1:1 to obtain the mixed cell suspension without observable intercellular assembly.

To trigger cell assembly, we selectively introduced FA to the surface of HL60 cells[15,51] by HRP-AptH-based APCL in the mixed cell suspension using DP as the labeling molecules, followed by washing and then reaction with N_3-modified FA (N_3-FA). After washing away unbound and endogenous FA, intercellular assembly of HeLa and HL60 cells was observed by CLSM imaging and FCM analysis after 30 min of incubation (Figure 5B), whereas little cell aggregation was observed in the group without APCL. These results demonstrate that our method can successfully transform non-FA-expressing HL60 cells to a FA-modified state, resulting in the redirection of cell−cell assembly in mixed cell suspensions. Note that although there have been some studies on cell assembly programming, these methods rely heavily on individual modification of cells prior to mixing them.[15,51,52] To the best of our knowledge, our method is the first work to accomplish cell modification and assembly programming in a hybrid cell system.

Simultaneous Manipulation and Tracking of Cell Cluster Formation. The combination of multiplexed labeling capability of APCL and the mutually orthogonal characteristics of the labeling molecules (BP, DP, and TP) enables the multifunctional manipulation of living cells in complex systems. To demonstrate this, we designed a cellular recruitment and tracking system consisting of two types of suspension cells and one type of adherent cells: two non-FA-expressing suspension cells, target HL60 and nontargeted Jurkat T cells, formed a mixed cell suspension; HeLa cells with high FAR expression formed an adhesive cell layer (Figure 5C). In their native states, HeLa cells cannot recruit either of these suspension cells. We attempted to selectively introduce N_3-FA on HL60 cells by APCL of DP to guide their targeted adhesion to HeLa cells. At the same time, APCL of TP was used to introduce the fluorescent tetrazine-Cy3 (Tz-Cy3) on HL60 cells to visualize the recruitment results.

We used HRP-AptH-based APCL to simultaneously label DP and TP on the cells, washed the cells, and treated the cell suspension with N_3-FA and Tz-Cy3. After washing the cells again, the cell suspension was allowed to incubate with the HeLa adhesion layer for 30 min. At this point, HL60 (Cy3-labeled, red) and Jurkat T (DiD prestained, green) cells could be seen in CLSM images. However, after washing the cell samples with PBS, only HL60 cells remained on the HeLa cell layer (Figure 5D). As a control, cells without APCL treatment were unable to be recruited to the HeLa adhesion layer, suggesting that HL60 adhesion on HeLa cells was dependent on the installed FA. We also calculated the number of clusters formed by 1 HeLa cell and 1, 2, 3, 4, 5, and ≥6 HL60 cells based on the imaging data (Figure 5E). The results showed that the cell cluster composed of one HeLa cell and one HL60 cell was dominant (37.3%), and the proportion of higher-order cell clusters decreased with the increase of the number of HL60 cells in the cluster.[15,51] These results confirm the advantage of using APCL for multifunctional manipulation of target cells in mixed cell systems.

Cell-Selective Neoglycosylation on Living Cells. We next explored the feasibility of APCL to directly assemble more complex biomolecules, represented by carbohydrates, on specific living cells. There are abundant glycan-modified conjugates in mammalian cell membranes, including glycoproteins and glycolipids. These sugars not only affect the structure, properties, and functions of the modified proteins/lipids but also act as major mediators of cellular response to the external environment.[56,57] On living cells, despite advances in metabolic oligosaccharide engineering[58−60] and chemoenzymatic methods[61−63] to label or edit certain glycan structures, the development of rapid, robust, and cell-compatible methods for *in situ* (neo-) glycosylation of diverse endogenous amino acids represents a grand challenge in glycoscience. This will expand the regulatory mechanisms of sugars on biological functions and provide a new prospect for cell engineering. Thus, by fabricating carbohydrate-modified

https://doi.org/10.1021/jacs.2c11150
J. Am. Chem. Soc. 2023, 145, 5092−5104

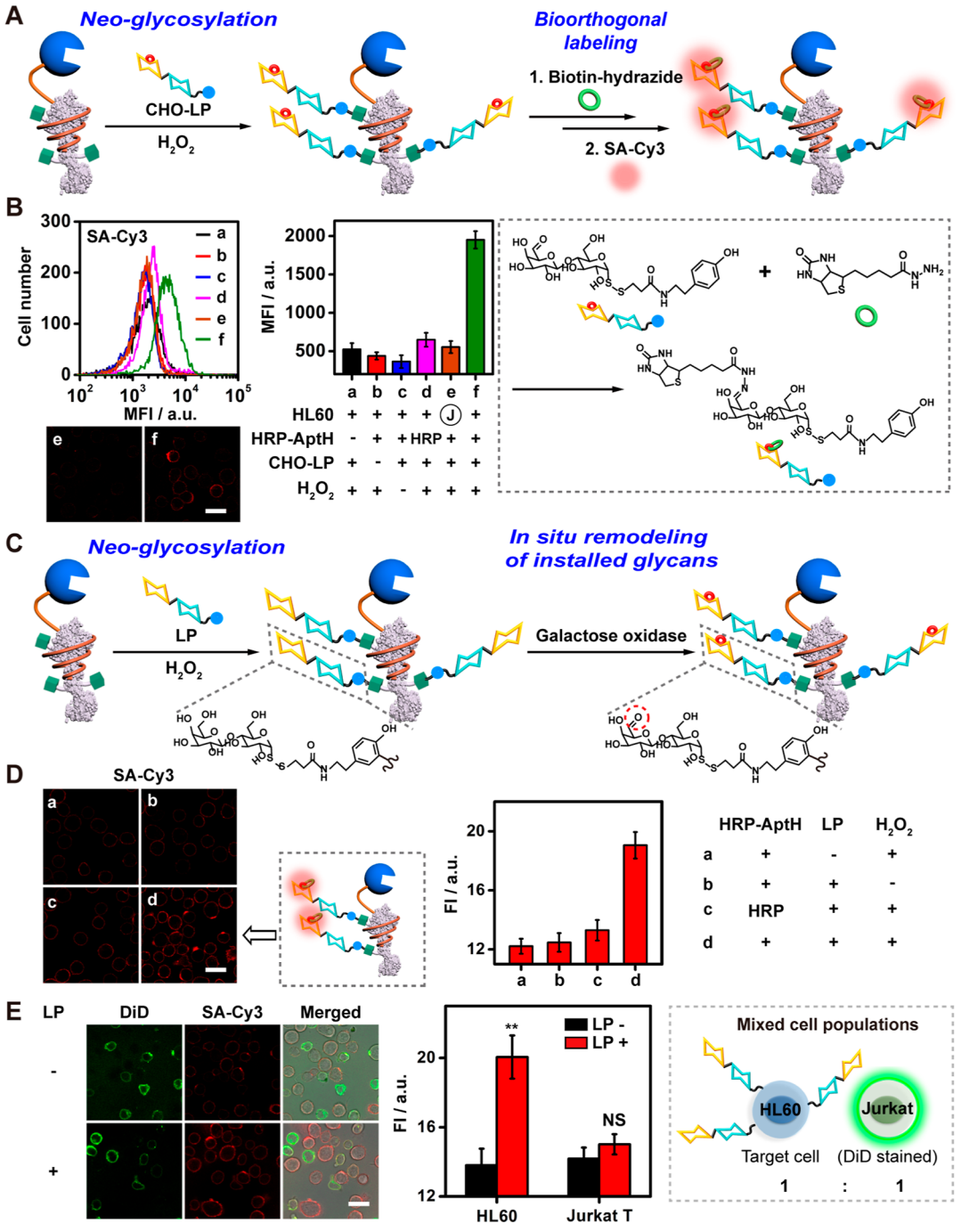

Figure 6. APCL-based neoglycosylation of living cells. (A) Schematic illustration of the APCL-mediated CHO-LP labeling and subsequent biotin-hydrazide ligation and SA-Cy3 staining. (B) FCM analysis (upper left) and CLSM imaging (bottom left) of CHO-LP on HL60 cells undergoing different combinations of treatments. MFI of SA-Cy3 obtained from FCM data are also shown (right). Jurkat T cells were used to replace HL60 cells to perform APCL of CHO-LP in (e). (C) Scheme of APCL-mediated LP labeling and GAO-mediated oxidation of installed LP. (D) CLSM imaging of the LP on HL60 cells after different combinations of treatments. LP was fluorescently labeled by GAO oxidation, biotin-hydrazide ligation, and SA-Cy3 staining (left). The FI of SA-Cy3 from images is also shown (right). (E) APCL-mediated LP labeling of HL60 cells in a mixed cell suspension (HL60 + Jurkat T, 1:1). CLSM images and FI of SA-Cy3 are shown. Scale bars: 20 μm. The images are representative of three individual experiments, and data are presented as mean ± SD, $n = 3$. $^{**}p < 0.01$ by student's t-test.

tyramine as a substrate, we exploited APCL to develop a neoglycosylation method for *in situ* reconfiguration of glycocalyx on living cells.

To demonstrate this, we synthesized lactose phenol (LP) *via* a modified method (Scheme S3).[64] The structures of intermediates and final products were confirmed by ^{1}H NMR, ^{13}C NMR, and high-resolution mass spectrometry (Figures S25−S30). Subsequently, CHO-LP was prepared by oxidizing the hydroxyl group at the C-6 position of LP to an aldehyde group by galactose oxidase.[65] We then performed APCL-mediated CHO-LP labeling followed by fluorescence visualization using the reaction between bioorthogonal aldehyde groups and biotin-hydrazine and subsequent SA-Cy3 binding (Figures 6A,B and S31, S32).[66] As expected, a

https://doi.org/10.1021/jacs.2c11150
J. Am. Chem. Soc. 2023, 145, 5092−5104

distinct fluorescent signal was visible on the cell surface. However, when any component of the labeling system was absent or HRP was substituted for HRP-AptH, only the background fluorescence signal was observed, indicating that CHO-LP was successfully covalently attached to the cell membrane. The fact that nontargeted Jurkat T cells could not be labeled proved that this operation was cell-selective.

This is the first report of *in situ* neoglycosylation using proximity covalent labeling. The proposed method is rapid, operationally simple, compatible with living cells, and requires no prior chemical modification or genetic intervention of cells. More importantly, newly introduced sugars will be attached to electron-rich amino acids represented by tyrosine on the surface of living cells. This is in contrast to the typical pattern of protein glycosylation, that is, asparagine-linked (*N*-linked) and serine-/threonine-linked (*O*-linked) glycosylation. Although tyrosine glycosylation also occurs in nature, such as tyrosine-*O*-glycosides found in glycogenin[67] and certain prokaryotic surface-layer glycoproteins,[68] it is less common. Our proposed method offers an opportunity to explore the effects of neoglycosylation of unnatural sites on protein and cellular functions. We also substituted LP for CHO-LP to install lactose on cell membrane proteins. The newly introduced sugar epitopes on the cell surface can be recognized by GAO *in situ*, as indicated by an increased fluorescent signal after BH labeling and incubation with SA-Cy3 (Figure 6C,D). This experiment demonstrates that APCL-based neoglycosylation can realize cascade glycoengineering of cell membranes. We further performed HRP-AptH-based APCL in a mixture of HL60 and Jurkat T (DiD stained) cells using LP or CHO-LP as the labeling molecules (Figures 6E and S33). As expected, only the target HL60 cells showed significant fluorescence of Cy3 (red), thus achieving cell-selective remodeling of the glycan layer in complex mixed systems.

CONCLUSIONS

We design an APCL platform for selectively customizing target cell surface molecules to program cell function and behavior in complex multicellular systems. Apt recognition, the high reactivity rate, and the short lifetime of the reaction intermediates ensure the cellular selectivity of the labeling process in mixed cell suspensions. The catalytic properties of APCL transform an Apt-based recognition event into multiple ultrafast enzymatic catalytic labeling on target cells, so this method has excellent cell discrimination ability. Most importantly, APCL allows the simultaneous installation of multiple functional moieties on target cells and is therefore a powerful tool for manually redirecting intercellular assembly and performing multifunctional cell manipulation. The method can be used on a variety of labeling molecules, and in particular, we demonstrate the applicability to sugar-modified phenol. We thus present a method for rapid neoglycosylation at nonclassical sites on the surface of living cells. We believe that our proposed method will be useful for the study of cell behavior and intercellular communication and has strong potential applications in immunotherapy, tissue engineering, and stem cell homing.

ASSOCIATED CONTENT

Supporting Information

The Supporting Information is available free of charge at https://pubs.acs.org/doi/10.1021/jacs.2c11150.

Experimental procedures and characterization results (PDF)

AUTHOR INFORMATION

Corresponding Author

Lin Ding − *State Key Laboratory of Analytical Chemistry for Life Science, School of Chemistry and Chemical Engineering, Nanjing University, Nanjing 210023, China; Chemistry and Biomedicine Innovation Center (ChemBIC), Nanjing University, Nanjing 210023, China;* orcid.org/0000-0001-5381-3484; Email: dinglin@nju.edu.cn

Authors

Yuna Guo − *State Key Laboratory of Analytical Chemistry for Life Science, School of Chemistry and Chemical Engineering, Nanjing University, Nanjing 210023, China; Medical Science and Technology Innovation Center, Shandong First Medical University, Jinan 250117, China*

Nan Wang − *State Key Laboratory of Analytical Chemistry for Life Science, School of Chemistry and Chemical Engineering, Nanjing University, Nanjing 210023, China*

Yihong Zhong − *State Key Laboratory of Analytical Chemistry for Life Science, School of Chemistry and Chemical Engineering, Nanjing University, Nanjing 210023, China*

Wei Li − *State Key Laboratory of Analytical Chemistry for Life Science, School of Chemistry and Chemical Engineering, Nanjing University, Nanjing 210023, China*

Yiran Li − *State Key Laboratory of Analytical Chemistry for Life Science, School of Chemistry and Chemical Engineering, Nanjing University, Nanjing 210023, China*

Guyu Wang − *State Key Laboratory of Analytical Chemistry for Life Science, School of Chemistry and Chemical Engineering, Nanjing University, Nanjing 210023, China*

Yunyan Yao − *State Key Laboratory of Analytical Chemistry for Life Science, School of Chemistry and Chemical Engineering, Nanjing University, Nanjing 210023, China*

Yue Shi − *State Key Laboratory of Coordination Chemistry, School of Chemistry and Chemical Engineering, Nanjing University, Nanjing 210023, China*

Liusheng Chen − *State Key Laboratory of Analytical Chemistry for Life Science, School of Chemistry and Chemical Engineering, Nanjing University, Nanjing 210023, China*

Xiaojian Wang − *Institute of Advanced Synthesis, School of Chemistry and Molecular Engineering, Nanjing Tech University, Nanjing 211816, China*

Huangxian Ju − *State Key Laboratory of Analytical Chemistry for Life Science, School of Chemistry and Chemical Engineering, Nanjing University, Nanjing 210023, China;* orcid.org/0000-0002-6741-5302

Complete contact information is available at: https://pubs.acs.org/10.1021/jacs.2c11150

Author Contributions

#Y.G., N.W., and Y.Z. contributed equally.

Notes

The authors declare no competing financial interest.

ACKNOWLEDGMENTS

We gratefully acknowledge support from the National Natural Science Foundation of China (21974067 and 22274073), Fundamental Research Funds for the Central Universities (021414380502 and 2022300324), and the State Key

Laboratory of Analytical Chemistry for Life Science (5431ZZXM2204).

REFERENCES

(1) Belardi, B.; Son, S.; Felce, J. H.; Dustin, M. L.; Fletcher, D. A. Cell-cell interfaces as specialized compartments directing cell function. *Nat. Rev. Mol. Cell Bio.* **2020**, *21*, 750−764.

(2) Liu, Z.; Xie, X.; Huang, Z.; Lin, F.; Liu, S.; Chen, Z.; Qin, S.; Fan, X.; Chen, P. R. Spatially resolved cell tagging and surfaceome labeling via targeted photocatalytic decaging. *Chem* **2022**, *8*, 2179−2191.

(3) Chang, X.; Zhang, C.; Lv, C.; Sun, Y.; Zhang, M.; Zhao, Y.; Yang, L.; Han, D.; Tan, W. Construction of a multiple-aptamer-based DNA logic device on live cell membranes via associative toehold activation for accurate cancer cell identification. *J. Am. Chem. Soc.* **2019**, *141*, 12738−12743.

(4) Stegle, O.; Teichmann, S. A.; Marioni, J. C. Computational and analytical challenges in single-cell transcriptomics. *Nat. Rev. Genet.* **2015**, *16*, 133−145.

(5) Papalexi, E.; Satija, R. Single-cell RNA sequencing to explore immune cell heterogeneity. *Nat. Rev. Immunol.* **2018**, *18*, 35−45.

(6) Custódio, C. A.; Mano, J. F. Cell surface engineering to control cellular interactions. *ChemNanoMat* **2016**, *2*, 376−384.

(7) Shi, P.; Wang, Y. Synthetic DNA for cell-surface engineering. *Angew. Chem., Int. Ed.* **2021**, *133*, 11684−11695.

(8) Jia, H. R.; Zhang, Z.; Fang, X.; Jiang, M.; Chen, M.; Chen, S.; Gu, K.; Luo, Z.; Wu, F. G.; Tan, W. Recent advances of cell surface modification based on aptamers. *Mater. Today Nano.* **2022**, *18*, 100188.

(9) Gartner, Z. J.; Bertozzi, C. R. Programmed assembly of 3-dimensional microtissues with defined cellular connectivity. *Proc. Natl. Acad. Sci. U.S.A.* **2009**, *106*, 4606−4610.

(10) Dutta, D.; Pulsipher, A.; Luo, W.; Yousaf, M. N. Synthetic chemoselective rewiring of cell surfaces: generation of three-dimensional tissue structures. *J. Am. Chem. Soc.* **2011**, *133*, 8704−8713.

(11) Cachat, E.; Liu, W.; Martin, K. C.; Yuan, X.; Yin, H.; Hohenstein, P.; Davies, J. A. 2- and 3-dimensional synthetic large-scale de novo patterning by mammalian cells through phase separation. *Sci. Rep.* **2016**, *6*, 20664.

(12) Chao, G.; Wannier, T. M.; Gutierrez, C.; Borders, N. C.; Appleton, E.; Chadha, A.; Lebar, T.; Church, G. M. helixCAM: A platform for programmable cellular assembly in bacteria and human. *Cells* **2022**, *185*, 3551−3567.

(13) Li, H.; Wang, M.; Shi, T.; Yang, S.; Zhang, J.; Wang, H. H.; Nie, Z. A DNA-mediated chemically induced dimerization (D-CID) nanodevice for nongenetic receptor engineering to control cell behavior. *Angew. Chem., Int. Ed.* **2018**, *57*, 10226−10230.

(14) Park, J.; Andrade, B.; Seo, Y.; Kim, M. J.; Zimmerman, S. C.; Kong, H. Engineering the surface of therapeutic "living" cells. *Chem. Rev.* **2018**, *118*, 1664−1690.

(15) Li, J.; Xun, K.; Zheng, L.; Peng, X.; Qiu, L.; Tan, W. DNA-based dynamic mimicry of membrane proteins for programming adaptive cellular interactions. *J. Am. Chem. Soc.* **2021**, *143*, 4585−4592.

(16) Prasad, V. Tisagenlecleucel—the first approved CAR-T-cell therapy: implications for payers and policy makers. *Nat. Rev. Clin. Oncol.* **2018**, *15*, 11−12.

(17) Wenzislava, C.; Caragea, A. E.; Goldstein, R. S.; Berleth, T. Glow in the dark: fluorescent proteins as cell and tissue-specific markers in plants. *Mol. Plant* **2021**, *5*, 794−804.

(18) Kim, H.; Skinner, D. J.; Glass, D. S.; Hamby, A. E.; Stuart, B. A. R.; Dunkel, J.; Riedel-Kruse, I. H. 4-bit adhesion logic enables universal multicellular interface patterning. *Nature* **2022**, *608*, 324−329.

(19) Roybal, K. T.; Lim, W. A. Synthetic immunology: hacking immune cells to expand their therapeutic capabilities. *Annu. Rev. Immunol.* **2017**, *35*, 229.

(20) Singh, J.; Petter, R. C.; Baillie, T. A.; Whitty, A. The resurgence of covalent drugs. *Nat. Rev. Drug Discovery* **2011**, *10*, 307−317.

(21) Kim, H.; Shin, K.; Park, O. K.; Choi, D.; Kim, H. D.; Baik, S.; Lee, H.; Kwon, S.-H.; Yarema, K. J.; Hong, J.; Hyeon, T.; Hwang, N. S. General and facile coating of single cells via mild reduction. *J. Am. Chem. Soc.* **2018**, *140*, 1199−1202.

(22) Li, Q.; Chen, Q.; Klauser, P. C.; Li, M.; Zheng, F.; Wang, N.; Li, X.; Zhang, Q.; Fu, X.; Wang, Q.; Xu, Y.; Wang, L. Developing covalent protein drugs via proximity-enabled reactive therapeutics. *Cell* **2020**, *182*, 85−97.e16.

(23) Rhee, H. W.; Zou, P.; Udeshi, N. D.; Martell, J. D.; Mootha, V. K.; Carr, S. A.; Ting, A. Y. Proteomic mapping of mitochondria in living cells via spatially restricted enzymatic tagging. *Science* **2013**, *339*, 1328−1331.

(24) Lam, S. S.; Martell, J. D.; Kamer, K. J.; Deerinck, T. J.; Ellisman, M. H.; Mootha, V. K.; Ting, A. Y. Directed evolution of APEX2 for electron microscopy and proximity labeling. *Nat. Methods* **2015**, *12*, 51−54.

(25) Li, J.; Han, S.; Li, H.; Udeshi, N. D.; Svinkina, T.; Mani, D. R.; Xu, C.; Guajardo, R.; Xie, Q.; Li, T.; Luginbuhl, D. J.; Wu, B.; McLaughlin, C. N.; Xie, A.; Kaewsapsak, P.; Quake, S. R.; Carr, S. A.; Ting, A. Y.; Luo, L. Cell-surface proteomic profiling in the fly brain uncovers wiring regulators. *Cell* **2020**, *180*, 373−386.

(26) Roux, K. J.; Kim, D. I.; Raida, M.; Burke, B. A promiscuous biotin ligase fusion protein identifies proximal and interacting proteins in mammalian cells. *J. Cell Biol.* **2012**, *196*, 801−810.

(27) Branon, T. C.; Bosch, J. A.; Sanchez, A. D.; Udeshi, N. D.; Svinkina, T.; Carr, S. A.; Feldman, J. L.; Perrimon, N.; Ting, A. Y. Efficient proximity labeling in living cells and organisms with TurboID. *Nat. Biotechnol.* **2018**, *36*, 880−887.

(28) Qin, W.; Cho, K. F.; Cavanagh, P. E.; Ting, A. Y. Deciphering molecular interactions by proximity labeling. *Nat. Methods* **2021**, *18*, 133−143.

(29) Kang, M. G.; Rhee, H. W. Molecular spatiomics by proximity labeling. *Acc. Chem. Res.* **2022**, *55*, 1411−1422.

(30) Robinson, P. V.; de Almeida-Escobedo, G.; de Groot, A. E.; McKechnie, J. L.; Bertozzi, C. R. Live-cell labeling of specific protein glycoforms by proximity-enhanced bioorthogonal ligation. *J. Am. Chem. Soc.* **2015**, *137*, 10452−10455.

(31) Li, L.; Chen, X.; Cui, C.; Pan, X.; Li, X.; Yazd, H. S.; Wu, Q.; Qiu, L.; Li, J.; Tan, W. Aptamer displacement reaction from live-cell surfaces and its applications. *J. Am. Chem. Soc.* **2019**, *141*, 17174−17179.

(32) Tivon, Y.; Falcone, G.; Deiters, A. Protein labeling and crosslinking by covalent aptamers. *Angew. Chem., Int. Ed.* **2021**, *60*, 15899−15904.

(33) Huang, Y.; Meng, L.; Nie, Q.; Zhou, Y.; Chen, L.; Yang, S.; Fung, Y. M. E.; Li, X.; Huang, C.; Cao, Y.; Li, Y.; Li, X. Selection of DNA-encoded chemical libraries against endogenous membrane proteins on live cells. *Nat. Chem.* **2021**, *13*, 77−88.

(34) Zhang, P.; Li, Y.; Yu, X.; Ju, H.; Ding, L. Switchable enzymatic accessibility for precision cell-selective surface glycan remodeling. *Chem. - Eur. J.* **2019**, *25*, 10505−10510.

(35) Kotani, N.; Gu, J.; Isaji, T.; Udaka, K.; Taniguchi, N.; Honke, K. Biochemical visualization of cell surface molecular clustering in living cells. *Proc. Natl. Acad. Sci. U.S.A.* **2008**, *105*, 7405−7409.

(36) Rees, J. S.; Li, X.-W.; Perrett, S.; Lilley, K. S.; Jackson, A. P. Selective proteomic proximity labeling assay using tyramide (SPPLAT): a quantitative method for the proteomic analysis of localized membrane-bound protein clusters. *Curr. Protoc. Protein Sci.* **2015**, *88*, 19−27.

(37) Joeh, E.; O'Leary, T.; Li, W.; Hawkins, R.; Hung, J. R.; Parker, C. G.; Huang, M. L. Mapping glycan-mediated galectin-3 interactions by live cell proximity labeling. *Proc. Natl. Acad. Sci. U.S.A.* **2020**, *117*, 27329−27338.

(38) Tamura, T.; Song, Z.; Amaike, K.; Lee, S.; Yin, S.; Kiyonaka, S.; Hamachi, I. Affinity-guided oxime chemistry for selective protein acylation in live tissue systems. *J. Am. Chem. Soc.* **2017**, *139*, 14181−14191.

https://doi.org/10.1021/jacs.2c11150
J. Am. Chem. Soc. 2023, 145, 5092−5104

(39) Geri, J. B.; Oakley, J. V.; Reyes-Robles, T.; Wang, T.; McCarver, S. J.; White, C. H.; Rodriguez-Rivera, F. P.; Parker, D. L., Jr.; Hett, E. C.; Fadeyi, O. O.; Oslund, R. C.; MacMillan, D. W. C. Microenvironment mapping via dexter energy transfer on immune cells. *Science* **2020**, *367*, 1091−1097.
(40) Oslund, R. C.; Reyes-Robles, T.; White, C. H.; Tomlinson, J. H.; Crotty, K. A.; Bowman, E. P.; Chang, D.; Peterson, V. M.; Li, L.; Frutos, S.; Vila-Perelló, M.; Vlerick, D.; Cromie, K.; Perlman, D. H.; Ingale, S.; Hara, S. D. O.; Roberts, L. R.; Piizzi, G.; Hett, E. C.; Hazuda, D. J.; Fadeyi, O. O. Detection of cell-cell interactions via photocatalytic cell tagging. *Nat. Chem. Biol.* **2022**, *18*, 850−858.
(41) Vong, K.; Tahara, T.; Urano, S.; Nasibullin, I.; Tsubokura, K.; Nakao, Y.; Kurbangalieva, A.; Onoe, H.; Watanabe, Y.; Tanaka, K. Disrupting tumor onset and growth via selective cell tagging (SeCT) therapy. *Sci. Adv.* **2021**, *7*, No. eabg4038.
(42) Xie, R.; Hong, S.; Feng, L.; Rong, J.; Chen, X. Cell-selective metabolic glycan labeling based on ligand-targeted liposomes. *J. Am. Chem. Soc.* **2012**, *134*, 9914−9917.
(43) Tuerk, C.; Gold, L. Systematic evolution of ligands by exponential enrichment: RNA ligands to bacteriophage T4 DNA polymerase. *Science* **1990**, *249*, 505−510.
(44) Tan, W.; Donovan, M. J.; Jiang, J. Aptamers from cell-based selection for bioanalytical applications. *Chem. Rev.* **2013**, *113*, 2842−2862.
(45) Huang, Q.; Huang, Q.; Pinto, R. A.; Griebenow, K.; Schweitzer-Stenner, R.; Weber, W. J. Inactivation of horseradish peroxidase by phenoxyl radical attack. *J. Am. Chem. Soc.* **2005**, *127*, 1431−1437.
(46) Ke, M.; Yuan, X.; He, A.; Yu, P.; Chen, W.; Shi, Y.; Hunter, T.; Zou, P.; Tian, R. Spatiotemporal profiling of cytosolic signaling complexes in living cells by selective proximity proteomics. *Nat. Commun.* **2021**, *12*, 71.
(47) Sefah, K.; Tang, Z. W.; Shangguan, D. H.; Chen, H.; Lopez-Colon, D.; Li, Y.; Parekh, P.; Martin, J.; Meng, L.; Phillips, J. A.; Kim, Y. M.; Tan, W. H. Molecular recognition of acute myeloid leukemia using aptamers. *Leukemia* **2009**, *23*, 235−244.
(48) Zhang, M.; Liu, H.; Chen, L.; Yan, M.; Ge, L.; Ge, S.; Yu, J. A disposable electrochemiluminescence device for ultrasensitive monitoring of K562 leukemia cells based on aptamers and ZnO@ carbon quantum dots. *Biosens. Bioelectron.* **2013**, *49*, 79−85.
(49) Sletten, E. M.; Bertozzi, C. R. Bioorthogonal chemistry: fishing for selectivity in a sea of functionality. *Angew. Chem., Int. Ed.* **2009**, *48*, 6974−6998.
(50) Zhang, D.; Zheng, Y.; Lin, Z.; Liu, X.; Li, J.; Yang, H.; Tan, W. Equipping natural killer cells with specific targeting and checkpoint blocking aptamers for enhanced adoptive immunotherapy in solid tumors. *Angew. Chem., Int. Ed.* **2020**, *59*, 12022−12028.
(51) Shi, P.; Zhao, N.; Lai, J.; Coyne, J.; Gaddes, E. R.; Wang, Y. Polyvalent display of biomolecules on live cells. *Angew. Chem., Int. Ed.* **2018**, *57*, 6800−6804.
(52) Li, J.; Xun, K.; Pei, K.; Liu, X.; Peng, X.; Du, Y.; Qiu, L.; Tan, W. Cell-membrane-anchored DNA nanoplatform for programming cellular interactions. *J. Am. Chem. Soc.* **2019**, *141*, 18013−18020.
(53) Guo, Z.; Zhang, L.; Yang, Q.; Peng, R.; Yuan, X.; Xu, L.; Wang, Z.; Chen, F.; Huang, H.; Liu, Q.; Tan, W. Manipulation of multiple cell-cell interactions by tunable DNA scaffold networks. *Angew. Chem., Int. Ed.* **2022**, *61*, No. e202111151.
(54) Stevens, M. M.; George, J. H. Exploring and engineering the cell surface interface. *Science* **2005**, *310*, 1135−1138.
(55) Nakagawa, F.; Kawashima, H.; Morita, T.; Nakamura, H. Water-soluble closo-dodecaborate-containing pteroyl derivatives targeting folate receptor-positive tumors for boron neutron capture therapy. *Cells* **2020**, *9*, 1615.
(56) Pinho, S. S.; Reis, C. A. Glycosylation in cancer: mechanisms and clinical implications. *Nat. Rev. Cancer* **2015**, *15*, 540−555.
(57) Schjoldager, K. T.; Narimatsu, Y.; Joshi, H. J.; Clausen, H. Global view of human protein glycosylation pathways and functions. *Nat. Rev. Mol. Cell Biol.* **2020**, *21*, 729−749.
(58) Mahal, L. K.; Yarema, K. J.; Bertozzi, C. R. Engineering chemical reactivity on cell surfaces through oligosaccharide biosynthesis. *Science* **1997**, *276*, 1125−1128.
(59) Laughlin, S. T.; Baskin, J. M.; Amacher, S. L.; Bertozzi, C. R. *In vivo* imaging of membrane-associated glycans in developing zebrafish. *Science* **2008**, *320*, 664−667.
(60) Wang, H.; Wang, R.; Cai, K.; He, H.; Liu, Y.; Yen, J.; Wang, Z.; Xu, M.; Sun, Y.; Zhou, X.; Yin, Q.; Tang, L.; Dobrucki, I. T.; Dobrucki, L. W.; Chaney, E. J.; Boppart, S. A.; Fan, T. M.; Lezmi, S.; Chen, X.; Yin, L.; Cheng, J. Selective *in vivo* metabolic cell-labeling-mediated cancer targeting. *Nat. Chem. Biol.* **2017**, *13*, 415−424.
(61) Liu, Z.; Li, J. P.; Chen, M.; Wu, M.; Shi, Y.; Li, W.; Teijaro, J. R.; Wu, P. Detecting tumor antigen-specific T cells via interaction-dependent fucosyl-biotinylation. *Cell* **2020**, *183*, 1117−1133.
(62) Chaubard, J. L.; Krishnamurthy, C.; Yi, W.; Smith, D. F.; Hsieh-Wilson, L. C. Chemoenzymatic probes for detecting and imaging fucose-α (1-2)-galactose glycan biomarkers. *J. Am. Chem. Soc.* **2012**, *134*, 4489−4492.
(63) Tang, F.; Zhou, M.; Qin, K.; Shi, W.; Yashinov, A.; Yang, Y.; Yang, L.; Guan, D.; Zhao, L.; Tang, Y.; Chang, Y.; Zhao, L.; Yang, H.; Zhou, H.; Huang, R.; Huang, W. Selective *N*-glycan editing on living cell surfaces to probe glycoconjugate function. *Nat. Chem. Biol.* **2020**, *16*, 766−775.
(64) Floyd, N.; Vijayakrishnan, B.; Koeppe, J. R.; Davis, B. G. Thiyl glycosylation of olefinic proteins: *S*-linked glycoconjugate synthesis. *Angew. Chem., Int. Ed.* **2009**, *48*, 7798−7802.
(65) Rannes, J. B.; Ioannou, A.; Willies, S. C.; Grogan, G.; Behrens, C.; Flitsch, S. L.; Turner, N. J. Glycoprotein labeling using engineered variants of galactose oxidase obtained by directed evolution. *J. Am. Chem. Soc.* **2011**, *133*, 8436−8439.
(66) Hui, J.; Bao, L.; Li, S.; Zhang, Y.; Feng, Y.; Ding, L.; Ju, H. Localized chemical remodeling for live cell imaging of protein-specific glycoform. *Angew. Chem., Int. Ed.* **2017**, *56*, 8139−8143.
(67) Mu, J.; Roach, P. J. Characterization of human glycogenin-2, a self-glucosylating initiator of liver glycogen metabolism. *J. Biol. Chem.* **1998**, *273*, 34850−34856.
(68) Zarschler, K.; Janesch, B.; Pabst, M.; Altmann, F.; Messner, P.; Schaffer, C. Protein tyrosine *O*-glycosylation—a rather unexplored prokaryotic glycosylation system. *Glycobiology* **2010**, *20*, 787−798.

https://doi.org/10.1021/jacs.2c11150
J. Am. Chem. Soc. 2023, 145, 5092−5104